

Control of Saccades with Model of Artificial 3D Biomimetic Eye

Carlos Aleluia
Instituto Superior Técnico
carlos.aleluia@tecnico.ulisboa.pt

Abstract—The human gaze control system is more complex than any robotic visual system ever built. One of its main challenges is dealing with the degrees of freedom problem: the six extra-ocular muscles provide the eye three degrees of freedom to rotate, while only two are necessary to gaze at any direction, controlling movements in a plane called Listing’s plane (LP). In this plane, the torsion of the eye is zero. Another distinctive trait of the saccadic system are its nonlinear dynamic properties, known as the *main sequence*. In this thesis we develop open-loop optimal control strategies that satisfy both criteria, finding the general optimization principles that unify them. These policies are tested on a model of a 3D biomimetic robot eye, whose kinematics were obtained using physics modelling of a previously built mechanical prototype. System identification procedures were employed to obtain a linear approximation of the nonlinear simulator within a small ocular range of the straight-ahead orientation. First, simpler approaches were tested, employing only minimization terms commonly used in literature. Even though the nonlinear dynamics were verified, the torsional scatter of the eye around LP ($\sigma = 1.8^\circ$) was higher than real data show ($\sigma = 0.6^\circ$). Then, the addition of extra cost terms (direct penalizations or minimization of the force) was studied, leading to the reduction of the scattering to 0.4° . Finally, the dependency of the orientation of LP to the geometry of the model was analysed.

Index Terms—biomimetic eye, Listing’s plane, *main sequence*, optimal control, physics modelling

I. INTRODUCTION

Even though robots are becoming increasingly complex and are already present in the daily lives of millions of people, no machine is more advanced than the human body. To execute even the most straightforward action, humans resort to sophisticated neural control that takes into account the degrees of freedom and the dynamic properties of the end effectors used to accomplish the task. The human eyes are one illustration of this issue. To gaze at any direction, only two degrees of freedom need to be specified: the azimuth and elevation angles. In fact, when building robotic eyes, engineers commonly account only for two rotations in each eyeball: horizontal and vertical. However, in the human visual system, there are six extraocular muscles controlling each eye, generating three degrees of freedom to rotate the eyeball (each eye is free to rotate around every axis in a 3D space). In the oculomotor system, for goal-directed eye movements, the orientations the eye assumes are constrained from three degrees of freedom to the minimum required (two) by Donders’ law, which states that the remaining rotation parameter is unambiguously determined

by the other two. If the head is kept upright and the gaze fixed at infinity, this law can be even further constrained: axes describing all eye orientations lie in a plane, when expressed by rotation vectors (this rule is known as Listing’s law) [1, 2]. One of the biggest debates regarding this subject in related literature is whether this behaviour rule is fully programmed by the brain, fully determined by the muscle properties or something in between [3].

The resolution of the extra-degree of freedom problem is not the only interesting property of oculomotor control. Experiments with humans and monkeys unveiled consistent nonlinear dynamic properties, such as the relationship between amplitude, duration and peak velocities in the saccadic system, known as the *main sequence* [4]. Other properties that are characteristic of a non-linear system are the skewness of velocity profiles for increasing saccade amplitudes and the stretching of gaze components in the case of oblique eye movements [5, 6].

The application of these strategies in a realistic hardware implementation is of critical importance not only because it will help to create more efficient gaze-control systems for robots but also because its control may lead to a better understanding and enlightenment of the neural fundamentals behind the referred dynamic properties. A more complete comprehension of the gaze control system may also help repair certain eye disorders such as impaired vision in the future [7].

The primary objective of this work is to create a saccadic optimal control system for a model of an artificial biomimetic eye. For this system, it is essential not only to control saccades according to Listing’s law (exhibiting only 2 degrees of freedom), but also to understand the nature of the empirical non-linear dynamic observed in the human eye relations that may or may not be observed for the resultant saccades. Thus, it is necessary to find the general optimization principles that unify both criteria and their relative importance. After attaining a functioning saccadic system, it is also interesting to analyse how the previously obtained results vary if changes occur in the geometry of the robotic eye or in the optimization terms. This will help deepen the analysis of which factors play the most determinant roles and exactly how they affect the normal behaviour of the model.

II. BACKGROUND

A. Eye Muscles and Orientation

Six muscles outside the eye, therefore called extraocular muscles, control its movement with exceptional accuracy and speed. The existence of six extraocular muscles would provide, in theory, six degrees of freedom to move the eyeball (three for translation and three for rotation). However, the mechanical enclosure inhibits almost any translation [8]. When one of the extraocular muscles exerts its tension, a torque is applied on the eyeball, which causes it only to rotate. Further, because muscles can only pull, and not push, they are paired two by two and they generate three degrees of freedom for rotations.

To describe eye orientations in 3D it is convenient to define a head-fixed reference frame from which to measure the three-dimensional rotation to the current eye position. This reference is usually defined as the orientation the eye exhibits with the head kept upright and looking straight-ahead (marked by the $+x$ axis). Positive torsion is clockwise (rotation about $+x$ axis), positive vertical movement is downward ($+y$ axis), and a positive horizontal movement is leftward ($+z$ axis). There are many different ways to represent 3D rotations: the most frequently proposed and employed ones in oculomotor literature are quaternions and rotation vectors [1].

B. Eye Orientation Rules

If the eye is fixating on a specific target, the object's position determines the gaze direction but does not specify the amount of ocular torsion about the line of sight. In this sense, theoretically, the eye could rotate any amount about the line of sight. However, the orientation of the rotating eye is not arbitrary: the movement of the eye is constrained by certain rules which remove the extra degree of freedom. These principles, Donders' and Listing's laws were formulated based on psychophysical observations and experiments.

Donders' law states that the torsional eye position is uniquely determined by the gaze direction (horizontal and vertical components), independently on the way the eye reached such an orientation. Thus, Donders' law states that the eye orientation has in fact only two degrees of freedom, rather than three.

Listing's law can be seen as a further specification of Donders' law, quantitatively defining the amount of torsion. In fact, Listing's law states that, when the head is fixed and the optical axes are parallel (gazing at far space), there is an eye orientation called primary position such that the eye assumes only the set of orientations that can be reached from the primary position by a single rotation about an axis in a plane [9]. This plane is orthogonal to the line of sight when the eye is in the primary position, and it is called Listing's plane. If the chosen reference frame is coincident with the primary position, and eye orientations are represented by a rotation vector $\mathbf{r} = (r_x, r_y, r_z)$, then Listing's law can be formulated simply as:

$$r_x = 0. \quad (1)$$

Listing's Law has later been verified through many experiments with monkeys and humans. In these experiments, the subject is seated with the head kept still and the eye orientations are recorded across many movements [10]. The results of one such experiment can be seen in figure 1. Observing the frontal view, it is clear that the subject looked all across the horizontal-vertical visual field (with about 30° range in each direction). However, the side and top view show that these eye orientations lie in a well-defined plane with virtually zero torsion.

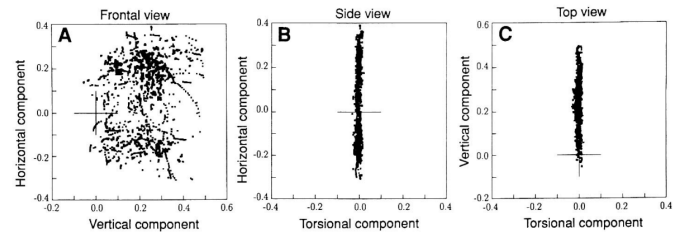


Fig. 1: Listing's law for eye positions in a monkey. All eye orientations lie in a well-defined plane, which is perpendicular to the torsional direction, thus defining the primary position (whose orientation is represented by a cross). The center of the oculomotor range is, in this case, downwards from the primary position. The axis correspond to the components of the rotation vectors: r_x (torsional), r_y (vertical) and r_z (horizontal). The units are half radians [10].

C. Nonlinear Dynamic Properties

In primates, there exists a consistent relationship between amplitude, duration and peak velocity of saccadic eye movements. These relationships, known as the *main sequence*, betray a non-linearity in the saccadic system, that is, the saccadic pulse controller must be non-linear [4]. Duration increases almost in a linear way for saccades bigger than a few degrees. It is important to realize that a linear system would have constant duration, and thus even a straight-line relationship is indicative of a nonlinear controller policy. Regarding the peak velocity, it is similarly related in a quasi-linear manner to saccadic amplitude up to nearly 20 degrees, after which it reaches a soft saturation limit and does not increase as much for bigger amplitudes [4].

Furthermore, the *main sequence* relations are not the only evidence of non-linearity in the pulse controller. The skewness of saccadic velocities is also a manifestation of non-linearity in the saccadic control system [5]. There is also evidence that eye trajectories are straight (saccades are represented by rotations about a single axis of rotation). This leads to the property of component stretching, which also demonstrates how the pulse generator is not only non-linear but also vectorial.

D. State of the Art

Some studies have focused on the mechanical versus neural hypotheses regarding the origins of Listing's law. Theoretical works have proven through models and mechanical

experiments that it is possible to obtain Listing’s behaviour (with results comparable with empirical data) solely based on the proper placement of insertion points and pulleys of the six extraocular muscles [11, 12]. Despite this, clinical evidence seems to suggest that Listing’s law is implemented by some sort of neural mechanism: failure of Listing’s law for general eye and head movements, during sleep, near-viewing and vestibular ocular reflexes; partial restoration of Listing’s behaviour in people with palsies that do not have a central brainstem origin [9]; and the active correction of small errors of Listing’s law by the saccadic system [13].

Recent theoretical studies suggest that the non-linear dynamic properties of saccadic eye movements reflect a deliberate optimization strategy. Following this line of thought, several studies have used optimal control theory as a framework to explain the *main sequence*. Some studies suggest that the neural fundamentals behind saccades have evolved to optimize the trade-off between time and accuracy, while others state that the *main sequence* can also be obtained by applying the minimum effort rule, according to which is assumed that the eye and head motor commands keep saccade duration as small as possible while minimizing the magnitude of the control signals.

III. METHODOLOGY

The methodology followed in this work can be seen in the diagram of figure 2, pictured in a simplified way. Analysing the image, the methodology contains 4 stages: first, a numerical, non-linear simulator is created based on a mechanical prototype, using physics modelling; then, the non-linear simulator is approximated by a linear model using system identification procedures; third, the identified model is used to compute the input sequence that optimizes the control of a specific saccade; finally, this input sequence is given to the nonlinear simulator, obtaining the results to be analysed later on.

A. Simulator

The simulator was based on a mechanical prototype (seen in figure 3) that was designed and tested in the context of the same project, as a first experiment in constructing a biomimetic 3D robotized system that needed to cope with the degrees of freedom problem. Even though reasonably good results were obtained regarding its static control, it had some problems in its dynamics. [14].

The main limitations that the model exhibited were:

- Low dynamic friction (underdamped system);
- High static friction (deadzone);
- Imperfect measurements (drift and noise).

In simulation, all these limitations are easy to eliminate. Furthermore, the use of a numerical simulator also eases the process of testing: in a mechanical model, it is very challenging to ensure identical conditions such as calibration for every trial, whereas a simulated system will always start in the same initial configuration. Also, it allows one to experiment on the influence of other parameters which on a real prototype would

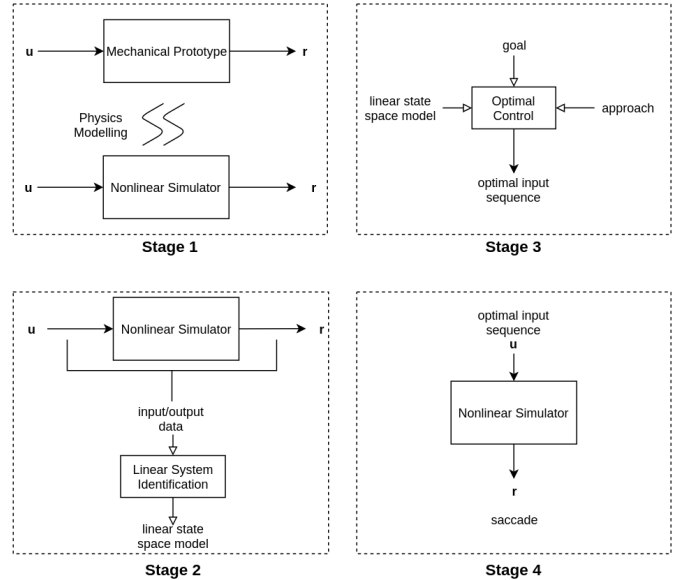


Fig. 2: Diagram representing the different stages in this work. The flow is divided into four parts: (1) creation of the simulator based on the mechanical prototype; (2) linear identification of the non-linear simulator; (3) optimal control of saccades, using the previously found model; (4) applying the optimal input sequence to the simulator.



Fig. 3: Previously built biomimetic 3D eye model. It is composed of a supportive green eye mounted on a ball joint sustained on a tripod. The eye is connected to six elastics (representing the six extraocular muscles) and controlled by three motors that pull the endpoints of those elastics (commanding, thus, only each pair of antagonist muscles) [14].

be rather difficult, as the relative positions of motor endpoints and pulleys.

The input for the simulator is $\mathbf{u} = (u_1, u_2, u_3)$, representing the three different motor angular positions, in degrees. The output is given by $\mathbf{r} = (r_x, r_y, r_z)$, the three components of the rotation vector representing the orientation of the eye. The simulator is built over Newton’s second law for rotation [15]:

$$\sum_j \tau_j = I\alpha, \quad (2)$$

where τ_j are the external torques applied to the rigid rotational

body, I is the inertia tensor and α is the angular acceleration over the three rotational axes.

The simulator computes the torques in a purely geometrical way, representing coordinates, velocities and accelerations as 3D vectors in space expressed in the world reference frame, whose origin is placed in the centre of rotation (the ball joint). A schematic on the required computations can be found in figure 4 for a generic elastic, where the geometry of the problem and the variables involved are more easily understood.

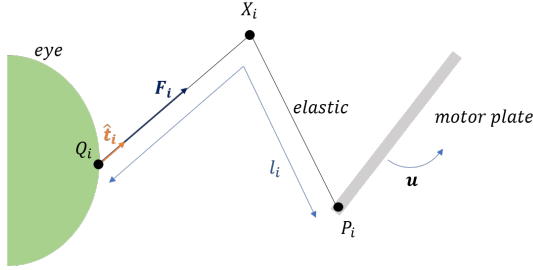


Fig. 4: Geometric schematic of the variables involved in the computation of the forces exerted on the eyeball for a single elastic. The represented variables are the following: P_i is the insertion point of the elastic on the motor plate; Q_i is the insertion point of the elastic in the eyeball; X_i is the intermediate ring where the elastic has to pass through; l_i is the total length of the elastic; F_i is the force exerted; \hat{t}_i is the direction of the force.

The elastic's insertion points on the motor plates are represented by P_i , corresponding to the coordinates in space of the points where the elastics are tied, expressed relative to the centre of rotation. Using simple trigonometrical relations, these coordinates can be easily written as functions of \mathbf{u} . Similarly, the coordinates of the elastic's insertion points on the eyeball, represented by Q_i , can be written as functions of the actual orientation of the eye, \mathbf{r} . Having these functions, it is easy to compute the current positions of both endpoints of the elastics, which can be used for calculating the forces F_i (all six elastics were modelled as simple springs whose tension F_i at the end is given by Hooke's law). Knowing the forces F_i applied in the eyeball and the points where they were exerted, Q_i , the torques are obtained by their cross product (see figure 5).

Once the torques exerted on the rigid body are known, the angular acceleration α can be computed by solving the linear equation (2), given that the inertia tensor is a constant for each time interval of the simulation. Then it is necessary to integrate the angular acceleration into angular velocity and obtain the change in orientation from one interval to another (using a first order differential equation for quaternions, see figure 5). Once the new orientation is computed, it is necessary to update the insertion points on the eye Q_i and the inertia tensor I (using the constant inertia tensor described in the eye reference frame I^0 , see figure 5). For both, it is necessary to convert the quaternion to a rotation matrix R .

A simplified diagram of the simulator, containing all the described steps, can be seen in figure 5. The simulator was implemented in Simulink, a toolbox from Matlab [16]. It is important to note that the simulator is nonlinear. For instance, the functions that compute P_i (insertion points on the motors) for a given input depend on trigonometric functions (sin and cos). This means that the model can only be well approximated by a linear system around a given operating point, and outside that region is expected to have large errors. Also, the pulling directions of the elastics change as the eye rotates, leading the gains between inputs and outputs to depend on the operating point. Thus, it is impossible to predict exactly the output based solely on the inputs.

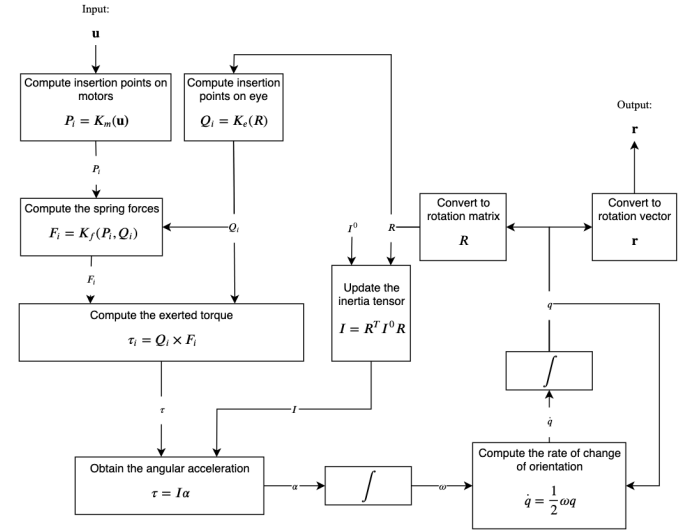


Fig. 5: Simplified diagram of functioning of the simulator. Each block contains a brief description of its purpose and a mathematical equation representing its operation.

B. Linear System Identification

In this process, corresponding to stage 2 of figure 2, one goes from experimental data to a mathematical model, learning the dynamical equations from observed input and output signals [17].

The system identification procedure needs four basic elements:

- The experimental input and output data;
- A collection of candidate models;
- A criteria to fit
- Validation of the identified model

The first step in the identification of the linear system which approximates the simulator is to define the type of input signal to be used in the generation of the experimental data. A 180 s long PRBS signal, uncorrelated between the three motor inputs, was used. The first 120 s (which sums up to 2/3 of the whole duration) were used for training the system identification algorithm, while the remaining 60 s were exclusively used for testing and validation of the resultant quality of fit.

The type of candidate model chosen was a state-space model, which is a way to represent the relation between a set of inputs and a set of outputs through n^{th} order differential equations comprised within a single first order matrix differential equation. This way, the discrete time system representation is given solely by two equations:

$$\begin{aligned} \mathbf{x}_{i+1} &= \mathbf{A}\mathbf{x}_i + \mathbf{B}\mathbf{u}_i \\ \mathbf{r}_i &= \mathbf{C}\mathbf{x}_i + \mathbf{D}\mathbf{u}_i, \end{aligned} \quad (3)$$

The method used to fit the parameters of the model was the subspace method, which is known to provide numerically reliable state-space models for complex multivariable dynamical systems, directly from measured data [17].

As a measure of the quality of the identification, the normalized root mean square error (NRMSE) fitness value was computed, indicating how well simulated or predicted model response matches the measurement data:

$$NRMSE(\%) = 100 \left(1 - \frac{\|r - \hat{r}\|}{\|r - \bar{r}\|} \right), \quad (4)$$

where r is the validation data output, \hat{r} is the output of the identified system and \bar{r} is the mean value of r .

Even though the obtained linearization was not perfect, it was generally good. The torsional and vertical components exhibited NRMSE values above 80% and the horizontal fit was nearly flawless. It is important to note that the linearization would always produce errors since the simulator is highly non-linear, and the achieved fit was considered sufficiently satisfactory.

C. Optimal Control

Optimal control theory is the process of finding the control law for a dynamical system over a period of time such that the performance of the system is optimal according to a certain criterion. This optimality criterion is usually defined in terms of a cost functional, which is a function of the state variables (that describe the current state of the system) and control variables (inputs, for example). Thus, the optimal solution corresponds to the minimizing the cost functional concerning the inputs to be given to the system. As discussed before, many different types of cost functions were used in related studies, including distinct terms representing the accuracy or duration of the saccade, or the minimization of error and effort during the movement.

This optimal open-loop control problem can be mathematically represented as the solution of the following optimization:

$$\begin{aligned} \text{minimize} \quad & J(\mathbf{U}, p, \mathbf{Y}) = \sum_{\alpha} \lambda_{\alpha} J_{\alpha}(\mathbf{U}, p, \mathbf{Y}) \\ & \mathbf{U}, p \\ \text{subject to} \quad & \mathbf{x}_{i+1} = \mathbf{A}\mathbf{x}_i + \mathbf{B}\mathbf{u}_i \\ & \mathbf{r}_i = \mathbf{C}\mathbf{x}_i + \mathbf{D}\mathbf{u}_i, \quad i = 0, \dots, p \end{aligned} \quad (5)$$

where J is the total cost functional and the pair λ_{α} and J_{α} represent the relative weight and cost functional of each of the terms composing the total J . Regarding the variables of optimization, p is the duration of the saccade and \mathbf{U} and \mathbf{Y}

are the concatenation of inputs and outputs, respectively, from the beginning of the saccade until time p .

The purpose of applying optimal control to our problem is to study which terms in the cost function lead to the following properties:

- Control of saccadic movements such that all axes describing eye orientations lie on a plane (Listing's plane);
- Replication of the nonlinear dynamic properties of saccades (*main sequence* relations, skewness and stretching of velocity profiles).

1) *Classical Terms*: Different approaches can be tested, varying in the cost terms included in the cost function. The first three approaches are composed of the most important minimization terms, obtaining the best trade-off between orientation error (or accuracy), energy spent and duration of the saccade. These three cost terms, deemed classical, will be explained below.

The accuracy term is the most intuitive: the goal is to minimize the difference between the target direction and the actual gaze direction at the end of the saccade. This is done by penalizing deviations for the last two components of the rotation vector (vertical and horizontal), leaving the torsional component free. So, the accuracy term can be written as:

$$J_A(\mathbf{r}_p) = \|\Lambda_{gaze}(\mathbf{r}_p - \hat{\mathbf{r}})\|^2, \quad (6)$$

where $\hat{\mathbf{r}}$ is the target gaze direction and Λ_{gaze} is a matrix such that

$$\Lambda_{gaze} \mathbf{r} = \begin{bmatrix} 0 & 0 & 0 \\ 0 & 1 & 0 \\ 0 & 0 & 1 \end{bmatrix} \begin{bmatrix} r_x \\ r_y \\ r_z \end{bmatrix} = \begin{bmatrix} 0 \\ r_y \\ r_z \end{bmatrix}. \quad (7)$$

Regarding the energy cost, since the input is directly the rotation given to the motor plates, the power consumed is proportional to changes in \mathbf{u} (that is, related to velocity) rather than proportional to the input itself. So, the energy term can be expressed as:

$$J_E(\mathbf{U}) = \|\Delta \mathbf{U}\|^2, \quad (8)$$

where Δ is a matrix written by blocks of identities, such that

$$\Delta \mathbf{U} = \begin{bmatrix} I & 0 & \dots & 0 \\ -I & I & \dots & 0 \\ \vdots & \vdots & \ddots & \vdots \\ 0 & \dots & -I & I \end{bmatrix} \mathbf{U} = \begin{bmatrix} \mathbf{u}_0 \\ \mathbf{u}_1 - \mathbf{u}_0 \\ \vdots \\ \mathbf{u}_p - \mathbf{u}_{p-1} \end{bmatrix}. \quad (9)$$

Lastly, the duration term implements a penalization that increases with the saccade duration given by p . There were many different ways of defining it. The chosen expression was an hyperbolic discount of reward, because it has been verified to fit empirical data of how humans discount reward as a function of time [18]. This leads to a duration cost that is expressed by:

$$J_D(p) = \left(1 - \frac{1}{1 + \beta p} \right), \quad (10)$$

where β is the rate at which the reward decays. A large value of β indicates that the subject is more impulsive, meaning he

would rather take a smaller amount of reward now than wait for the larger amount.

Based on the three classical minimization terms, three different approaches can be considered, depending on which of the terms are included in the cost function. The only term which must be present at all times is the accuracy term, for, without it, the saccade will be ill-defined.

So, the classical approaches and corresponding functional J are:

- **AED**: optimizes accuracy, energy and duration:

$$J_{AED}(\mathbf{U}, p, \mathbf{Y}) = \lambda_A J_A(\mathbf{r}_p) + \lambda_E J_E(\mathbf{U}) + \lambda_D J_D(p); \quad (11)$$

- **AE**: optimizes accuracy and energy:

$$J_{AE}(\mathbf{U}, p, \mathbf{Y}) = \lambda_A J_A(\mathbf{r}_p) + \lambda_E J_E(\mathbf{U}); \quad (12)$$

- **AD**: optimizes accuracy and duration:

$$J_{AD}(\mathbf{U}, p, \mathbf{Y}) = \lambda_A J_A(\mathbf{r}_p) + \lambda_D J_D(p). \quad (13)$$

2) *Listing's Plane Terms*: In addition to the foregoing cost terms, it is also possible to include additional functionals that relate to Listing's behaviour. With these, the control of saccades is expected to be further constrained to a plane rather than having all three degrees of freedom for rotations. Two types of costs can be thought of when penalizing deviations from Listing's plane: for the whole trajectory or exclusively for the orientation attained at the end of the saccade. In both, Listing's plane must be presumed a priori: thus, the primary position was assumed to correspond to the straight-ahead orientation. This makes sense since, originally, the simulator is symmetrical.

When penalising deviations from Listing's plane only for the final orientation, the cost term to be considered can be written as:

$$J_{LJP \text{ target}}(\mathbf{r}_p) = \|\Lambda_{torsion} \mathbf{r}_p\|^2, \quad (14)$$

where $\Lambda_{torsion}$ is a matrix such that

$$\Lambda_{torsion} \mathbf{r} = \begin{bmatrix} 1 & 0 & 0 \\ 0 & 0 & 0 \\ 0 & 0 & 0 \end{bmatrix} \begin{bmatrix} r_x \\ r_y \\ r_z \end{bmatrix} = \begin{bmatrix} r_x \\ 0 \\ 0 \end{bmatrix}. \quad (15)$$

On the other hand, when the whole movement is evaluated with respect to Listing's plane, the cost term to be considered can be written as:

$$J_{LJP \text{ trajectory}}(\mathbf{Y}) = \left\| \begin{bmatrix} \Lambda_{torsion} \\ \Lambda_{torsion} \\ \vdots \\ \Lambda_{torsion} \end{bmatrix} \mathbf{Y} \right\|^2. \quad (16)$$

So, as Listing's restrictions are concerned, two new different approaches can be considered:

- **Target**: Only the final orientation is constrained to Listing's plane:

$$J_{target}(\mathbf{U}, p, \mathbf{Y}) = \lambda_A J_A(\mathbf{r}_p) + \lambda_E J_E(\mathbf{U}) + \lambda_D J_D(p) + \lambda_{LJP} J_{LJP \text{ target}}(\mathbf{r}_p); \quad (17)$$

- **Trajectory**: All points during the movement are constrained to Listing's plane:

$$J_{trajectory}(\mathbf{U}, p, \mathbf{Y}) = \lambda_A J_A(\mathbf{r}_p) + \lambda_E J_E(\mathbf{U}) + \lambda_D J_D(p) + \lambda_{LJP} J_{LJP \text{ trajectory}}(\mathbf{Y}). \quad (18)$$

3) *Force Term*: The previous approaches (the ones containing J_{LJP} terms) assume prior knowledge on Listing's plane, to constrain the movement to it. However, it may also be the case that Listing's plane is initially unknown. For example, if the positioning of the motors relative to the eye is not symmetrical, then it is not trivial to predict what will be the orientation of the primary position. One hypothesis is to consider the plane of possible orientations that minimize the effort in each motor, that is, the difference between the forces at each end of the motor plates. The biological analogue of this is to minimize tension in the extraocular muscles. By doing this, movements that were free to rotate torsionally become restricted by choosing the configuration that leads to less effort for a given target.

The relation between the force and the orientation is hard to model analytically. For that reason, an empirical approximation relating these two quantities was obtained by least-squares fitting of a quadratic form:

$$J_F \approx \mathbf{r}^T H_F \mathbf{r}. \quad (19)$$

A quadratic form was chosen because the dependency of force on orientation resembled quadratic behaviour. Data was gathered for a collection of different orientations and the best estimate H_F found.

The total functional for the approach that includes force minimization is:

$$J_{force}(\mathbf{U}, p, \mathbf{Y}) = \lambda_A J_A(\mathbf{r}_p) + \lambda_E J_E(\mathbf{U}) + \lambda_D J_D(p) + \lambda_F J_F(\mathbf{r}_p). \quad (20)$$

Only the last value of force was included in the cost term because it was enough to make the system choose a final configuration from the possible set (with different torsional values), and that partly constrained the whole movement as well. Furthermore, a minimal weight was given to this term, i.e., $\lambda_F \ll \lambda_A$. This is because the objective is that the force minimization only acts as a differentiating element between saccades ending in the same vertical and horizontal desired orientations, and never influence the final gaze direction components r_y and r_z .

IV. RESULTS

In this section, we present the experiments carried out and we show the corresponding results. Furthermore, before each test, the reasoning behind it and the experimental setup in which it was conducted are also thoroughly described.

A. Ocular Range

First of all, some tests were done to determine the ocular range of the biomimetic model. This is extremely important because we had to ensure the created simulator had 3 degrees

of freedom for rotations. Only this being valid can conclusions be taken regarding the control of saccades in Listing's Plane (only 2 degrees of freedom). For this purpose, random combinations of inputs (within a range of $\pm 45^\circ$) were given to the model and all eye orientations were sampled (including during the movement). Table I contains the range (maximum and minimum registered rotations, in degrees) for each of the components. As can be observed, the range is intrinsically

TABLE I: Absolute values of the ocular range in each of the orientation components.

Component	Min ($^\circ$)	Max ($^\circ$)
Torsional (r_x)	-28.51	29.13
Vertical (r_y)	-48.61	49.88
Horizontal (r_z)	-54.20	52.29

distinct for different axes. However, even though the range of the torsional component is smaller, its limits were around 30° away from the origin, which is a large amount of torsion nonetheless. Furthermore, r_x exhibited a standard deviation of 7.63° , which is much bigger than the experimental value of 0.6° in primates. So, the simulator has, in fact, 3 degrees of freedom for rotations.

B. Classical Approaches

After confirming the total degrees of freedom of the simulator, it is interesting to evaluate how well the created strategies abide Listing's law and to observe if they lead to a non-linear dynamic behaviour.

To analyse Listing's law, data was gathered for multiple saccades in sequence, recording the orientation of the eye throughout the movements. For that purpose, 1500 saccades were randomly generated according to a two-dimensional Gaussian distribution on the gaze direction components: vertical (r_y) and horizontal (r_z). Given the same set of random saccades, the optimal control strategies were applied for the approaches described so far, one at a time. Here, given the symmetry of the simulator, the primary position is assumed to be the straight-ahead orientation, meaning that Listing's plane is simply defined by $r_x = 0$ for all eye orientations (if the reference frame is coincident with the primary position). So, the scattering of the torsional component must be small. This aspect can be well represented by the standard deviation of r_x (mathematically expressed by σ_{r_x}).

Another important feature is that trajectories should be straight (since they are accomplished through rotation about a single axis). This condition may be characterized by the mean of all correlations of vertical and horizontal velocity profiles, represented by $\bar{\rho}_{v_y, v_z}$. This value should be close to one.

Regarding the nonlinear dynamics, three properties should be verified: the *main sequence* relations between duration, peak velocity and amplitude of saccades; skewness of velocity profiles; and stretching of components for oblique saccades. For the *main sequence*, the relations between duration, peak velocity and amplitude were studied for the set of all saccades

previously done. To analyse skewness, the velocity profiles of saccades with the same direction but scaled amplitude were inspected. Regarding stretching, the velocities of two saccades were examined: the first was a purely horizontal saccade; the second was an oblique saccade with the same horizontal component as the latter.

1) *AED*: Running all saccades using the AED approach (equation (11)), we obtained the results of figure 6. The set of all eye orientations are plotted in three different planes, similarly to what was done in figure 1.

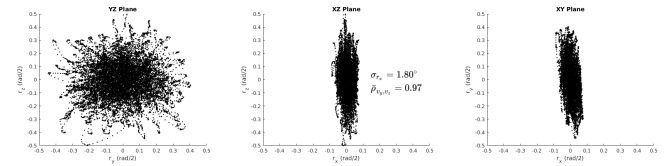


Fig. 6: Eye orientations for all saccades when using the AED approach (equation (11)).

As can be seen in figure 6, the model looked almost all across the visual field (about 40° range both in horizontal and vertical gaze directions in the YZ planes). Regarding the thickness of Listing's plane, using the AED approach led to a somewhat thick Listing's plane. Even so, σ_{r_x} is below 2° which is much smaller than the value presented in the ocular range experiment. Nevertheless, it exhibited almost perfect straightness of trajectories ($\bar{\rho}_{v_y, v_z}$ close to 1).

The equivalent *main sequence* plots can be seen in figure 7. Inspecting the images, it is possible to conclude that the *main sequence* relations are respected for the AED approach. In the shown plots, there are multiple directions for saccades. Naturally, distinct directions lead to slightly different cost terms and, so, to a different compromise between energy and time. This means that the duration plot actually contains multiple lines with different slopes, and the same happens for the peak velocity plot. To demonstrate this specific occurrence, beyond representing the data for all saccades in black, certain directional saccades are also represented in different colours: red (purely horizontal), green (purely vertical) and blue (oblique).

The skewness and stretching tests can also be found in figure 7. As for skewness, it is verified how velocity profiles skew more as the amplitude grows. Regarding stretching, the horizontal component of the oblique saccade (red line) is stretched relative to the purely horizontal saccade (blue line) to match the time evolution of the vertical component of the oblique saccade (yellow line). So, all three nonlinear dynamic properties hold.

2) *AE*: Using the AE approach, the equivalent results can be found in figures 8 (Listing's law) 9 (nonlinear dynamics).

The AE approach (optimizing only accuracy and energy) produced better results regarding the thickness of Listing's plane, leading to a plane with similar scattering as recorded in empirical experiments in primates. However, $\bar{\rho}_{v_y, v_z}$ was low in this case, which indicates that the rotations were not about

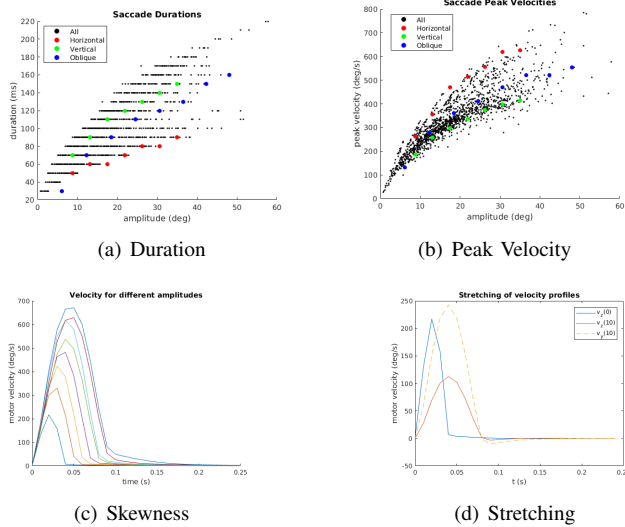


Fig. 7: Dynamics of the system when using the AED approach.

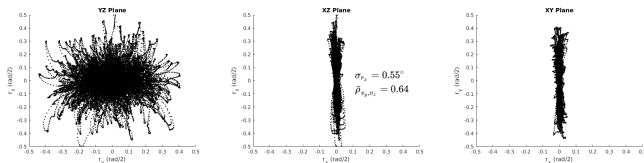


Fig. 8: Eye orientations for all saccades when using the AED approach (equation (12)).

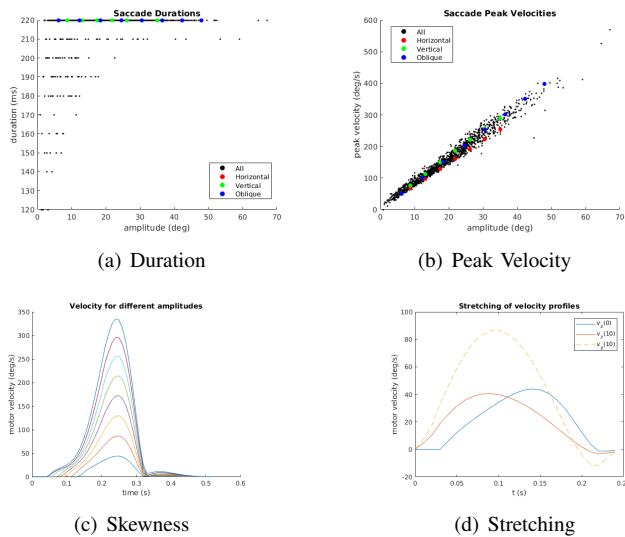


Fig. 9: Dynamics of the system when using the AE approach.

a single axis of rotation. This is because, given the symmetry of the system, the model is energetically more efficient near the origin. Thus, and since the duration of saccades is not a concern, the optimization will choose trajectories that always pass through the origin before arriving on the specified target gaze direction, regardless of the time it takes. This is clear by analysing the XZ plane of figure 8: the orientations always

go through the center of the ocular range. Furthermore, in this approach, the nonlinear dynamic properties relations no longer hold. Saccade duration is almost always (more than in 90% of the cases) the maximum allowed by the optimizer. About the peak velocities, they grow linearly with the amplitude instead of saturating. Regarding skewness, velocity profiles are almost just scaled versions of each other as the amplitude grows. Stretching is also not verified: the velocities do not change that much for oblique saccades.

3) *AD*: Using the AD approach, the equivalent results can be found in figures 10 (Listing's law) 11 (nonlinear dynamics).

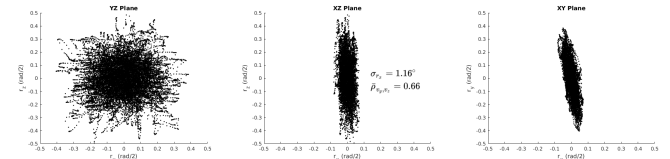


Fig. 10: Eye orientations for all saccades when using the AED approach (equation (13)).

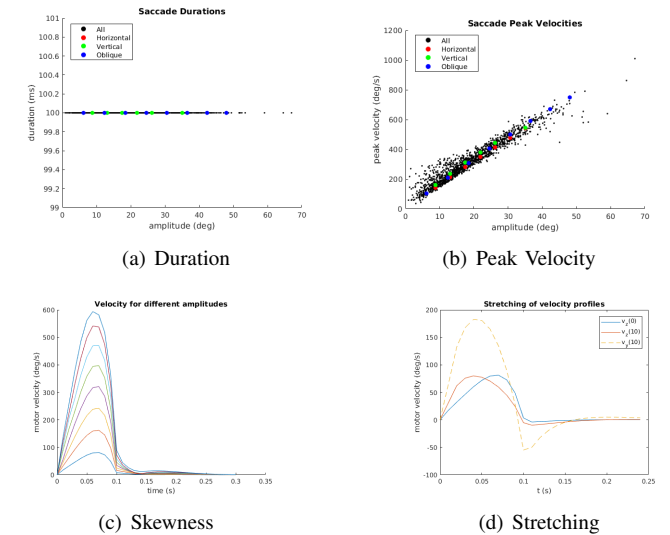


Fig. 11: Dynamics of the system when using the AD approach.

Applying the AD minimization functional produced a thinner plane than AED, but still with higher scattering than AE. The straightness of trajectories was not that good either. It is important to note that optimizing time is somewhat incomplete: without any constriction on the inputs given throughout the movement, the chosen values for U will always be the largest possible to obtain the desired gaze direction in the minimum time allowed. So, this type of trajectory is unrealistic and fails when applied to the non-linear simulator. Similarly to what occurred in the AE approach, none of the non-linear dynamic properties were found using the AD approach. The only difference relative to the previous case is that saccade durations were always the least permitted (since the duration term increases with time), instead of being the longest allowed.

So, to conclude this analysis, it was observed that, from the set of classical approaches presented, only the one that

contains every term (AED) seems to obtain the same dynamic properties as the eye exhibits.

C. Additional Listing's Constraints

Next, the effect of the additional Listing's Plane cost terms was evaluated. The main flaw of the AED approach was that the obtained Listing's plane was somewhat thick. So, these other two alternatives have the purpose of further restricting the movement to a plane. However, the possible benefits that may be obtained must be evaluated knowing that the inclusion of these extra cost terms is somewhat artificial, specially stating that the eye should be in Listing's plane during the complete trajectory. Furthermore, they require the specification of the orientation of the primary position a priori. Regarding this, the primary gaze of direction was assumed to be the straight-ahead orientation, given the symmetry of the model. The recorded orientations for the target and trajectory approaches can be visualized in figure 12.

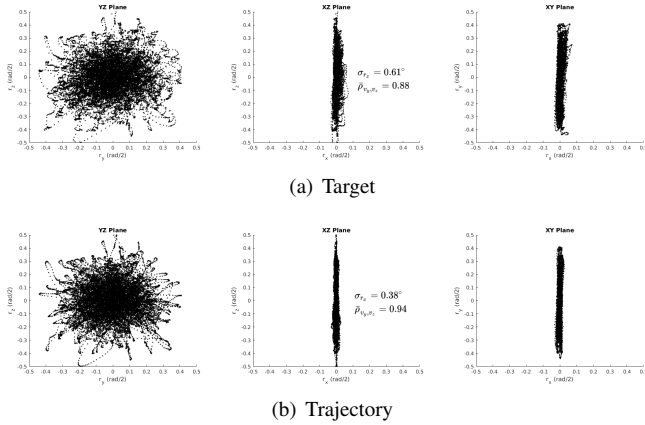


Fig. 12: Eye orientations for all saccades when using the two alternative approaches regarding the additional cost terms penalizing deviations from Listing's plane. Top row (a): the eye is penalised for deviations from Listing's plane at the end of the movement only. Bottom row (b): the eye should stay as close to Listing's plane as possible throughout the movement.

As can be observed, the addition of the extra terms greatly reduces the scattering of the plane. About the straightness of trajectories, neither approach has produced much worse results. Concluding, the two approaches with the additional Listing's plane terms improve the results significantly, but the difference between them was not critical.

D. Force Minimization

Lastly, the inclusion of a force term is studied as an alternative way to restrict the movement to be given in a certain plane. In this case, however, the plane is not initially assumed but rather discovered empirically with the data.

1) *Symmetrical Case*: This approach was first applied in the symmetrical case (the same model used for all the previous experiments) to find which is the plane of least force. The analysed variables were the same as before: σ_{r_x} to understand

the scattering of the plane and $\bar{\rho}_{v_y, v_z}$ to assess how straight the trajectories were. One extra variable was computed: the inclination of Listing's plane, in the XZ plane (represented by δ). It is useful to note that, in primates, the primary gaze of direction is not the straight-ahead orientation, but about 15° looking upwards. Translating to rotation vector notation, this means there is a tilt in the $r_x r_z$ plane, and a similar phenomenon could happen here.

The results of all orientations when carrying out the set of 1500 random saccades can be seen in figure 13.

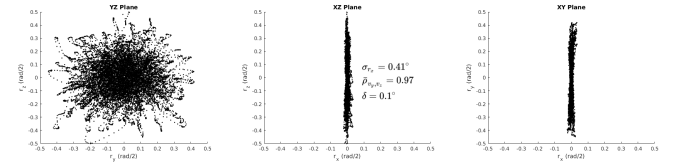


Fig. 13: Eye orientations for all saccades when using the force approach (equation (20)), applying it to a symmetrical model.

The inclusion of force minimization in the total functional produced extraordinarily good results: the scattering of Listing's plane was very small (less than what was obtained by real measurements) and the straightness was nearly perfect ($\bar{\rho}_{v_y, v_z} = 0.97$). Regarding the inclination of Listing's plane, the obtained result was $\delta = 0.1^\circ$, which means the plane is almost straight and thus defined approximately by $r_x = 0$. This is concordant with the assumption made for all the previous experiments: if the system is symmetrical with respect to the motor insertion points, then the primary position is simply the eye looking straight ahead. It is also relevant to note that the inclusion of the force term does not impact the nonlinear dynamic properties exhibited by the AED approach: the force term only restricts the final orientation of the movement. So, for this approach, both the *main sequence*, skewness and stretching were also observed.

2) *Asymmetrical Case*: After evaluating the performance of this new approach compared with the previous ones, it is also interesting to apply one of its main advantages: with the inclusion of a force term, the orientation of Listing's plane is also an output of testing with random saccades. This means it is possible to change certain aspects of the simulator and observe the impact it generates on the orientation of the primary position.

One of the variables whose influence is most interesting to study is the relative position of the motors to the eyeball. This is related to what occurs in the real eye: the insertion points to which the extra-ocular muscles pull are not directly behind the eyeball, but rather aligned obliquely. The relative position of the motors was, then, shifted upwards or downwards with respect to the centre of the ocular range. The variable used to characterize this offset was d_z , and it ranged from -8 cm to $+8\text{ cm}$, in steps of 2 cm at a time.

This empirical dependency between the offset d_z and the obtained δ is represented in figure 14. Examining the progression of the data, one can observe that the angle δ increases

almost linearly with the displacement d_z set in the simulator. Only the final point (corresponding to $d_z = 8 \text{ cm}$) seems to deviate by a small amount from the general tendency, with a practically constant slope.

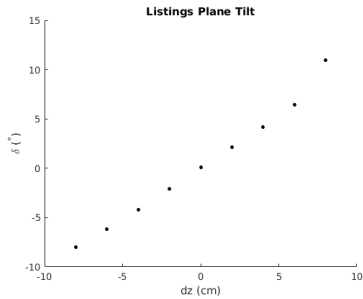


Fig. 14: Dependency of the tilt of Listing’s plane δ with the offset d_z in the motor insertion points for the analysed cases.

V. CONCLUSIONS

A. Discussion

Given the presented results, we conclude that, to obtain the non-linear dynamic properties that the real eye exhibits, both energy and duration need to be minimized for each saccade. Within this specific set, the classical approach to contain all three optimization terms (AED) led to planes with a substantial thickness (1.8° of scattering, as opposed to the empirical 0.6°). Some strategies were developed to further restrict the movement to a certain plane. Directly penalising deviations from Listing’s plane led to thinner planes than using the AED approach but exhibited somewhat curved trajectories. Between the two alternatives, it is preferable to demand that only the final orientation is inside a plane than enforcing it for the whole trajectory because it is more natural. Regarding the second type of strategy (minimizing force), it led to the shortening of Listing’s plane ($\sigma_{r_x} = 0.4^\circ$) and maintained the straightness of trajectories ($\bar{\rho}_{v_y, v_z} = 0.97$). So, adding these better results to the fact that minimizing force is more intuitive and realistic, and does not require a priori knowledge about the orientation of Listing’s plane, we conclude that the force strategy is preferable.

B. Future Work

Regarding possible future work to be done, it is relevant to find a global model, that is, a model that approximated the non-linear system in other regions (the linear system found was only valid around the straight-ahead orientation). One possibility is to use different linear models in different areas of operation and join these in a single non-linear model. A more biomimetic approach to noise is also interesting: in biological systems, the noise is usually proportional to the magnitude of the input signal. In this work, noise was eradicated and energy was minimized. However, other studies have been presented where it is precisely the presence of multiplicative noise that leads to the *main sequence* relations. Truthfully, in the real human eye, the inertia is small enough so that energy minimization

is not expected to be a determinant factor. Then, the inclusion of proportional noise can allow a more thorough exploration of this subject and, more specifically, of alternatives to the presented cost terms. Furthermore, the implementation of these optimal control strategies in a real robotic prototype (where truly unexpected situations will occur in the environment) is the real critical test of their validity.

REFERENCES

- [1] T. Haslwanter, “Mathematics of three-dimensional eye rotations,” *Vision research*, vol. 35, no. 12, pp. 1727–1739, 1995.
- [2] K. Hepp, “On listing’s law,” *Communications in Mathematical Physics*, vol. 132, no. 1, pp. 285–292, 1990.
- [3] A. J. Van Opstal, “200 years franciscus cornelis donders,” *Strabismus*, vol. 26, no. 4, pp. 159–162, 2018.
- [4] A. T. Bahill, M. R. Clark, and L. Stark, “The main sequence, a tool for studying human eye movements,” *Mathematical Biosciences*, vol. 24, no. 3-4, pp. 191–204, 1975.
- [5] A. Van Opstal and J. Van Gisbergen, “Skewness of saccadic velocity profiles: a unifying parameter for normal and slow saccades,” *Vision research*, vol. 27, no. 5, pp. 731–745, 1987.
- [6] W. King, S. Lisberger, and A. F. Fuchs, “Oblique saccadic eye movements of primates,” *Journal of neurophysiology*, vol. 56, no. 3, pp. 769–784, 1986.
- [7] J. van Opstal, “Orient erc adv grant nr. 693400,” [Online]. Available: http://www.mbfys.ru.nl/johnvo/OrientWeb/orient_1.html, 2019, Accessed on October 19th 2019.
- [8] R. S. Snell and M. A. Lemp, *Clinical anatomy of the eye*. John Wiley & Sons, 2013.
- [9] A. M. Wong, “Listing’s law: clinical significance and implications for neural control,” *Survey of ophthalmology*, vol. 49, no. 6, pp. 563–575, 2004.
- [10] A. J. van Opstal, K. Hepp, B. Hess, D. Straumann, and V. Henn, “Two-rather than three-dimensional representation of saccades in monkey superior colliculus,” *Science*, vol. 252, no. 5010, pp. 1313–1315, 1991.
- [11] G. Cannata, M. D’Andrea, and M. Maggiali, “Design of a humanoid robot eye: models and experiments,” *2006 6th IEEE-RAS International Conference on Humanoid Robots*, pp. 151–156, 2006.
- [12] D. Biamino, G. Cannata, M. Maggiali, and A. Piazza, “Mac-eye: a tendon driven fully embedded robot eye,” *5th IEEE-RAS International Conference on Humanoid Robots, 2005.*, pp. 62–67, 2005.
- [13] J. Van Opstal, K. Hepp, Y. Suzuki, and V. Henn, “Role of monkey nucleus reticularis tegmenti pontis in the stabilization of listing’s plane,” *Journal of Neuroscience*, vol. 16, no. 22, pp. 7284–7296, 1996.
- [14] M. Lucas, “Construction and characterization of a biomimetic robotic eye model with three degrees of rotational freedom: A testbed for neural control of eye movements,” M. S. thesis, Instituto Superior Técnico, Lisboa, 2017.
- [15] S. J. Ling, J. Sanny, W. Moebis, G. Friedman, S. D. Druger, A. Kolakowska, D. Anderson, D. Bowman, D. Demaree, E. Ginsberg *et al.*, *University Physics Volume 1*. OpenStax, 2016.
- [16] MathWorks, “Simulink,” [Online]. Available: <https://www.mathworks.com/products/simulink.html>, 2019, Accessed on September 5th 2019.
- [17] L. Ljung, *System Identification: Theory for the User*. Prentice Hall PTR, 1999.
- [18] R. Shadmehr, J. J. O. De Xivry, M. Xu-Wilson, and T.-Y. Shih, “Temporal discounting of reward and the cost of time in motor control,” *Journal of Neuroscience*, vol. 30, no. 31, pp. 10507–10516, 2010.